ACS NANO

www.acsnano.org

Article

Magnetic Field Tunable Raman Scattering and Zone-Folding Phonons in Two-Dimensional Magnet CrSBr

Junyang Chen,[‡] Mingqiang Gu,[‡] Xiaohua Wu, Shoujing Chen, Guangji Xing, Mengyuan Jia, Tiejun Huang, Hao Peng, Minghong Sun, Qihang Liu, Yanan Dai, and Mingyuan Huang[*]

Cite This: *ACS Nano* 2026, 20, 2655−2663

Read Online

ACCESS | Metrics & More | Article Recommendations | Supporting Information

ABSTRACT: The discovery of two-dimensional (2D) magnets has attracted significant attention in both fundamental research in low-dimensional physics and potential applications in spintronics. CrSBr, an A-type antiferromagnetic (AFM) van der Waals material with intralayer ferromagnetic (FM) order along the *b* axis, stands out as one of the most extensively studied 2D magnetic materials due to the strong coupling between its electronic structure and magnetic properties. Here, we demonstrate a deep connection between the magnetic order and Raman scattering of phonons in CrSBr. By applying a magnetic field along the easy axis, an abrupt change of Raman intensity is observed in the transition from the AFM to FM state for both bulk and few-layer CrSBr, which is attributed to the modification of the energy detuning between the excitation light and the near-resonant exciton. In addition, at the *a*-axis spin-canted state, we observe three strong zone-folding phonon modes of the three dominant A_g modes, which are absent at both AFM and FM states. Furthermore, we find that the FM magnetic order can introduce off-diagonal terms into the Raman tensors, which can dramatically modify the polarization patterns of the Raman modes and lead to different scattering intensities for the left and right circularly polarized light. Our findings underline the profound impact of the magnetic order on the Raman scattering intensity, activity of zone-folding phonons, and polarization properties in CrSBr and expand the scope of magneto-optical effects in 2D magnetic materials.

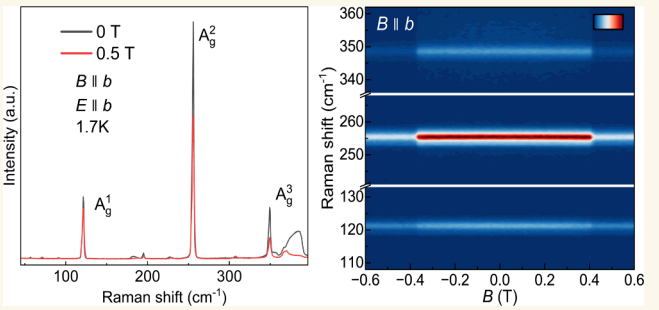

KEYWORDS: *2D magnets, Raman spectroscopy, zone-folding phonons, CrSBr, magneto-optical effect*

INTRODUCTION

The advent of 2D magnets has emerged as one of the most promising areas in condensed matter physics, offering an ideal platform to explore fascinating physical properties and potential applications in the two-dimensional limit,[1−9] including magnetic proximity effects,[10,11] quantum Hall effects,[12] moiré engineering,[13−15] and spintronics.[9,16,17] The recently discovered A-type AFM semiconductor CrSBr displays strong anisotropic magneto-transport[18−20] and relatively high air stability,[18,21] which is promising for potential spintronic applications. CrSBr possesses intrinsically coupled electronic, optical, and magnetic properties, which makes it an ideal platform to explore novel magneto-optical phenomena.[21] The recent experiments demonstrate quasi-1D exciton emission coupled with magnetic order,[21,22] magnon-exciton coupling,[23,24] and exciton polaritons.[25−27]

Due to the high sensitivity to symmetries of the crystal lattice, Raman spectroscopy is extensively used to probe both structural and magnetic phase transitions in 2D magnetic materials. For example, in CrI_3[28] and VI_3,[29] the strong magneto-Raman effect was demonstrated by the different scattering intensities to the left and right circularly polarized light; in $CrBr_3$[30] and $Cr_2Ge_2Te_6$,[31] the strong spin-phonon coupling was revealed by the anomalous phonon frequency variation near their Curie temperature; in CrI_3[32] and $MnBi_2Te_4$,[33] the Brillouin zone-folding Raman modes due to the magnetic order were observed. While previous Raman spectroscopy studies in CrSBr have reported the excitation wavelength-dependent polarization patterns of Raman modes and strong spin-phonon coupling,[34−37] the direct experimental study of the Raman spectrum under a magnetic field is still lacking.

In this work, we report a comprehensive study of the Raman spectrum of CrSBr under a magnetic field. By applying the magnetic field along the easy (*b*) axis, most of the Raman modes display a sudden intensity drop in bulk CrSBr at the transition from the AFM to FM state, which originates from the increase in the energy difference between the excitation light and the near-resonant B-exciton.[21,35,38,39] This Raman

Received: August 1, 2025
Revised: December 28, 2025
Accepted: December 29, 2025
Published: January 14, 2026

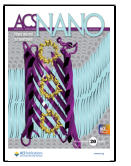

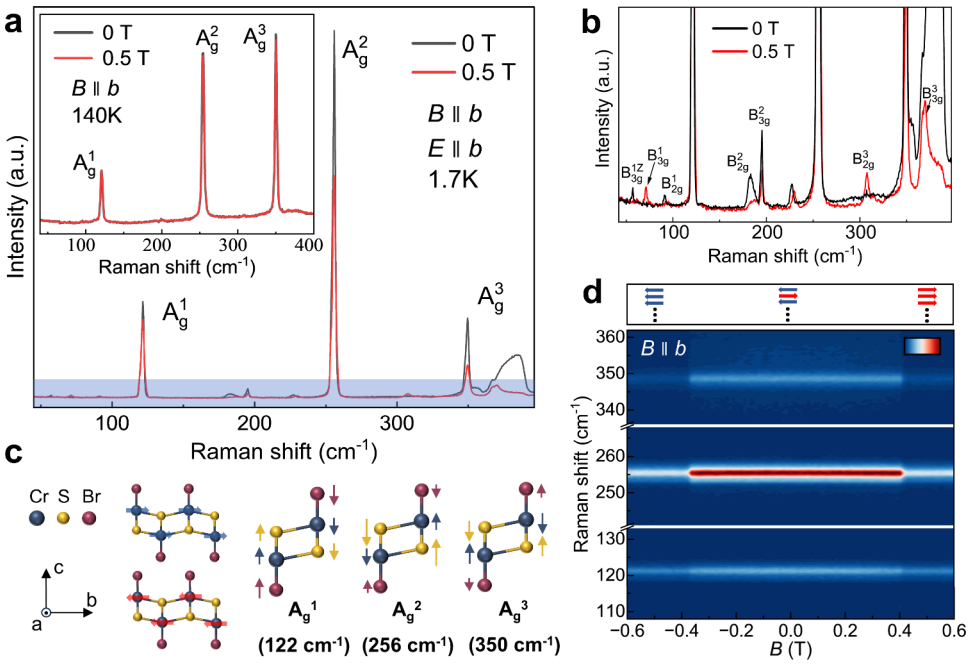

Figure 1. Raman spectra of bulk CrSBr under a magnetic field along the *b* axis. (a) Raman spectra of bulk CrSBr under a magnetic field of 0 (AFM, black) and 0.5 T (FM, red) at 1.7 K. Inset: Raman spectra were recorded under magnetic fields of 0 and 0.5 T at temperature above the T_N. (b) Close-up of the low-intensity part (blue shaded area) of the Raman spectrum in panel (a). (c) Schematic crystal structure of CrSBr and the atomic displacements of the A_g modes. (d) Evolution of the Raman spectra of the A_g modes with the applied magnetic field. The incident light was polarized along the *b* axis for all measurements in the figure.

intensity contrast can also be resolved for few-layer CrSBr, even for the metastable intermediate magnetic state. In addition, three zone-folding phonon modes from the A_g mode branches emerge in the Raman spectrum of CrSBr at the spin-canted state when the magnetic field is applied along the *a* axis, and these zone-folding phonon modes are Raman-inactive at AFM, FM, and *c*-axis canting states. Furthermore, the Raman tensors of the dominant A_g modes are derived by considering the magnetic order, and the off-diagonal terms are introduced for the FM state. By applying the magnetic field along the *c* axis, we observe dramatic modification of the polarization patterns for the A_g modes and different scattering intensities to the left and right circularly polarized light due to these off-diagonal terms.

RESULTS AND DISCUSSION

To study the impact of magnetic order on the Raman spectrum of CrSBr, we first performed the magneto-Raman measurements on bulk CrSBr with both the magnetic field and the polarization of the excitation light along the *b* axis at low temperature. Figure 1a displays the representative Raman spectra acquired under magnetic fields of 0 and 0.5 T. Three prominent A_g Raman modes are observed at 122, 256, and 350 cm^{-1} labeled as A_g^1, A_g^2, and A_g^3, respectively, and their atomic displacements are calculated by density functional theory (DFT) and presented in Figure 1c, which is consistent with the previous reports.[34−37] According to previous studies,[21,40,41] the magnetic order of bulk CrSBr is AFM at 0 T and will be polarized into FM at 0.5 T. Clearly, all three A_g phonon modes show significant intensity difference in Raman spectra at the AFM and FM states, while such intensity difference disappears for the same magnetic field in the paramagnetic state above T_N (≈132 K), as demonstrated in the inset of Figure 1a. These results indicate that the Raman intensity difference originates from the magnetic order of CrSBr rather than the external fields. To confirm this conclusion, the Raman measurement with a full sweep of the magnetic field is performed and Figure 1d displays the evolution of the Raman spectrum with the increasing magnetic field from −0.6 to 0.6 T. We can clearly see two abrupt intensity changes for all three A_g modes at critical fields of −0.38 and 0.42 T, while they are otherwise constant elsewhere. Obviously, these sudden intensity variations are directly related to magnetic order changes, which is further confirmed by our magneto-PL measurements in Figure S2 and previous reports.[21,40,41]

Besides the three A_g Raman modes, the magnetic order change also leads to a large intensity modification of the B_g and multiple-phonon modes.[35] Figure 1b shows the magnified low-intensity spectral region of Figure 1a, in which seven B_g phonon modes can be identified with the help of a DFT calculation. We note that these B_g Raman modes are typically forbidden in the backscattering geometry, and their appearance may be due to the convergence of the incident light by the objective. Similar to the A_g phonon modes, all of those B_g modes show magnetic-order-dependent Raman intensity. Specifically, most of the B_g (except the B_{3g}^1 and B_{2g}^3) phonon modes display a higher Raman intensity at the AFM state than at the FM state. In addition, the B_{3g}^1 mode at 74 cm^{-1} only shows up at the FM state, and with the disappearance of the B_{3g}^1 mode at the AFM state, a new peak at 54 cm^{-1} emerges. This new Raman mode is assigned as a zone-folding phonon mode of the B_{3g}^1 mode through the DFT calculation and labeled as the B_{3g}^{1Z}. This result is consistent with the previously reported temperature-dependent Raman study.[35]

According to previous reports, the characteristics of the Raman spectrum of CrSBr can be effectively modulated by the excitation wavelength via the resonance effect.[34,36] In our experiment, the excitation wavelength was fixed at 632.8 nm,

https://doi.org/10.1021/acsnano.5c13065
ACS Nano 2026, 20, 2655−2663

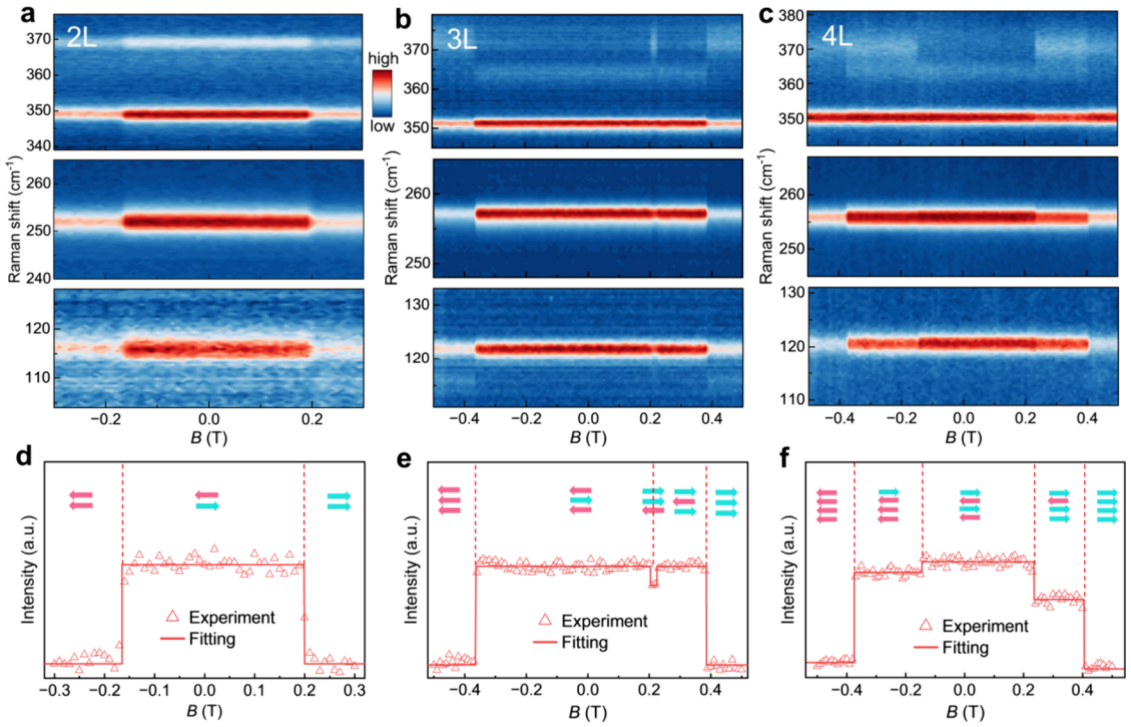

Figure 2. Raman spectra of a few-layer CrSBr under a magnetic field along the *b* axis. (a–c) Evolution of the Raman spectra of the A_g modes with the applied magnetic field for 2L (a), 3L (b), and 4L CrSBr (c). (d–f) Plots of the Raman intensity of the A_g^2 mode as a function of the applied field for 2L (d), 3L (e), and 4L CrSBr (f). The interlayer magnetic order is illustrated on the upper panels. The magnetic field is swept from negative to positive.

corresponding to a photon energy of 1.96 eV, which is close to the B-exciton energy (~1.8 eV) of bulk CrSBr at the AFM state.[21,35,38,39] By considering the energies of the studied phonons less than 400 cm^{-1} (~0.05 eV), both energies of the excitation and scattering photons are less than those of the B-exciton. When the magnetic order of bulk CrSBr is changed from the AFM to FM by an external field, the B-exciton energy displays a significant redshift,[21,38,39] which is further detuned from the energies of the excitation and scattering light. Through this resonance effect analysis, we expect Raman intensity to decrease for bulk CrSBr from the AFM to FM state, which is consistent with the clear intensity dropping for most of the phonons, as shown in Figure 1a,b. We note that some of the phonons (such as A_g^3) display inverse behavior in different measurement configurations, which might imply that the Raman scattering process of these phonons has other connections with the magnetic order besides the resonance effect (see the Supporting Information, S8 for more information).

To further investigate the impact of magnetic order on the Raman spectra, we next performed the layer-dependent magneto-Raman studies on 1–4L CrSBr samples, and their spin configurations were recently studied by various methods, such as PL, differential reflectance, and second harmonic generation (SHG).[21,40,42,43] For 1L CrSBr, the Raman spectrum shows no discernible change with the magnetic field (Figure S5a). Figure 2a presents the field-dependent Raman spectra of three A_g phonons for 2L samples, in which their intensities undergo two abrupt changes at −0.17 and 0.19 T, similar to bulk samples but with a less coercive field, and these changes are obviously related to the spin-flip transitions between the AFM and FM states. For 3L CrSBr, despite the fact that the spin-left (←→←) and spin-right (→←→) AFM states are spectrally indiscernible, we still observed a transient Raman intensity variation for a narrow range of the magnetic field around 0.23 T (Figure 2b,e). Based on our PL measurement (Figure S2) and previous report,[40,42] we conclude that this transient Raman feature originates from a metastable intermediate spin state of "←→→". Figure 2d,e plots the Raman intensities of the A_g^2 modes for the 2L and 3L CrSBr as a function of the magnetic field, with the spin-configuration schematics annotated by arrows in the upper panels.

Furthermore, the magneto-Raman data for 4L CrSBr are listed in Figure 2c. Through the Raman intensity contrast, we can easily identify the AFM state near the zero field, two FM states for the magnetic field of more than 0.4 T and less than −0.4 T, and two transitional states with one spin pointing in one direction and the other three spins pointing in the opposite direction between the AFM and FM states. Interestingly, two transitional states display different Raman intensities, which means that these two states are not equivalent for the Raman spectrum. With the help of the magneto-PL results and previous reports,[40,43,44] one of the transitional states is assigned as the opposite-direction spin in the surface layer and another for the inner layer. The intensity of the A_g^2 mode is extracted and plotted as a function of the magnetic field in Figure 2e, along with the spin configurations. In summary, our results establish Raman spectroscopy as an effective probe of detailed spin textures in bulk and few-layer CrSBr.

For bulk CrSBr, besides the AFM and FM states, its magnetic order can be tuned into a spin-canted state by applying a magnetic field along the intermediate (*a*) and hard (*c*) axes. Here, we turn to explore the impact of the canted magnetic order on the Raman spectra of CrSBr. Figure 3a

https://doi.org/10.1021/acsnano.5c13065
ACS Nano 2026, 20, 2655–2663

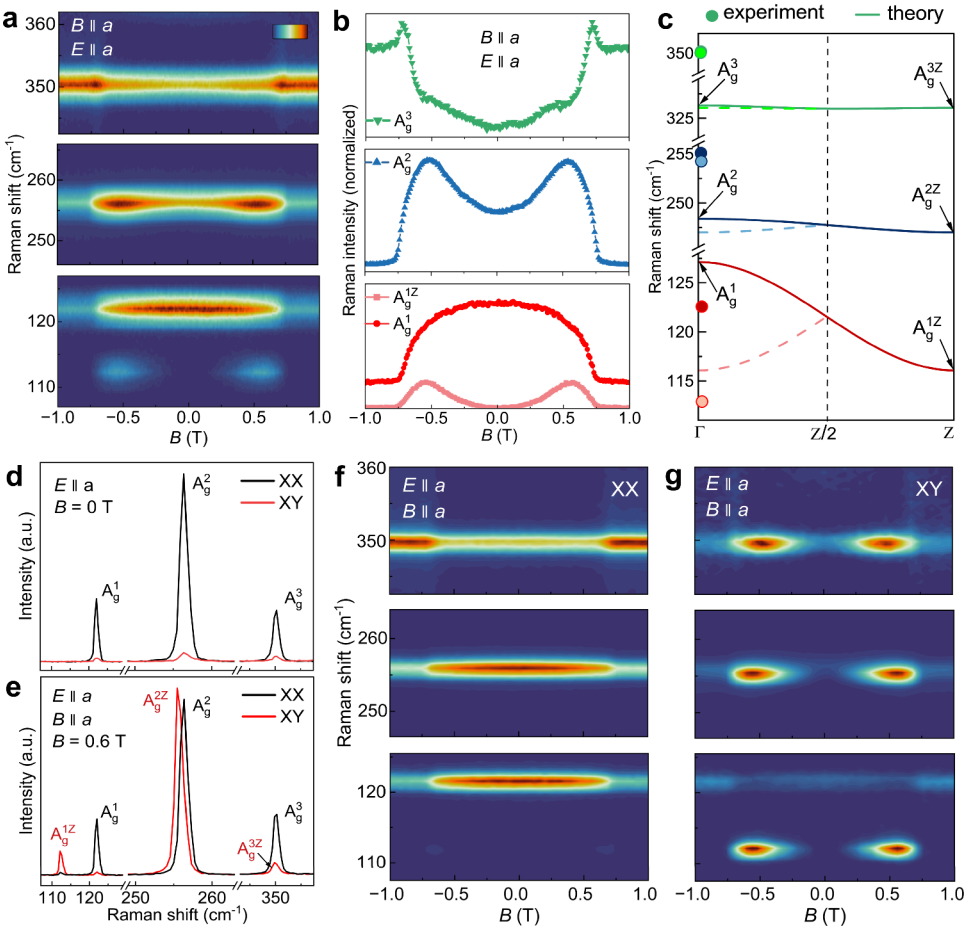

Figure 3. Raman spectra of the zone-folding phonon modes. (a) Evolution of the Raman spectra of the A_g modes with the applied magnetic field along the *a* axis. (b) Plot of the intensities of the Raman modes (A_g^1, A_g^2, A_g^3, and A_g^{1Z}) in panel (a) as a function of the magnetic field. (c) The DFT-calculated phonon dispersion of the A_g mode branches along the Γ-Z direction. The measured A_g and zone-folding phonon frequencies are denoted by the dark and light dots, respectively. (d, e) Linear polarization-resolved Raman spectra from both parallel (XX) and cross (XY) channels at 0 and 0.6 T. (f, g) Evolution of the polarization-resolved Raman spectra from the XX (f) and XY (g) channels with the applied magnetic field.

presents the Raman spectra as a function of the magnetic field along the *a* axis, with the excitation light polarized along the *a* axis (the results for the light polarized along the *b* axis are provided in the Supporting Information, S11). As the magnetic field increases (decreases), the A_g^1 (122 cm^{-1}) mode gradually loses its intensity until the saturation field, while the intensity of the A_g^2 (256 cm^{-1}) mode increases first and then undergoes a sharp decrease near the saturation field until reaching the saturation, and the behavior of the A_g^3 (350 cm^{-1}) mode is similar to the A_g^2, except its saturation intensity is higher than that of the initial state. Furthermore, a new peak (112 cm^{-1}) at the lower frequency side of the A_g^3 peak emerges gradually as the magnetic field increases and then quickly disappears as CrSBr reaches the FM state. The Raman intensities of the phonon modes mentioned above are plotted as a function of the magnetic field in Figure 3b.

To understand the anomalous field-dependent Raman scattering intensity of the A_g^2 and A_g^3 modes and the appearance of the new peak in the spin-canted states, we performed polarized magneto-Raman measurements. Figure 3f,g shows the evolution of the Raman spectra from both parallel (XX, Figure 3f) and cross (XY, Figure 3g) channels as the magnetic field sweeps from −1 to 1 T. In the XX channel, three A_g phonon modes display a normal gradual intensity change from the AFM to FM states, and the new Raman mode is absent. In the XY channel, the intensity variation of the Raman modes at around 256 and 350 cm^{-1} shows remarkable similarity with the new Raman mode at around 112 cm^{-1}, which indicates that the abnormal intensity behavior of the A_g^2 and A_g^3 modes originates from the overlap of the newly emerged modes with the old ones. To further confirm the new Raman modes, the Raman spectra from both XX and XY channels at 0 and 0.6 T are plotted in Figure 3d and Figure 3e, respectively, and about a 0.6 cm^{-1} frequency shift is observed for the Raman modes at around 256 cm^{-1} and about 0.15 cm^{-1} for the Raman modes at around 350 cm^{-1} (Supporting Information, S12). These newly emerged Raman modes in the XY channel are assigned as zone-folding phonon modes of the A_g branches due to the spin-canted magnetic order and labeled as A_g^{1Z}, A_g^{2Z}, and A_g^{3Z}.

To confirm our assignment of the zone-folding phonon modes, we performed DFT calculations for the phonon dispersion of CrSBr. We first consider the nonmagnetic primitive cell of CrSBr. There are six atoms in the primitive cell, leading to 15 optical phonon modes at the Γ-point, with three A_g modes. The calculated eigenvector of the A_g modes is displayed in Figure 1c, and the energy band of the A_g branches along the Γ-Z direction is plotted in Figure 3c. By considering the magnetic order of spin canting, the magnetic unit cell will be doubled along the *Z* direction, which will cause the zone boundary phonons to fold to the Γ point. From Figure 3c, the

https://doi.org/10.1021/acsnano.5c13065
ACS Nano 2026, 20, 2655−2663

Table 1. MSGs and Raman Tensors for AFM and FM-*a*, FM-*b*, and FM-*c* Configurations

	AFM	FM-*a*	FM-*b*	FM-*c*
MSG	P_anma	$Pmm'n'$	$Pmm'n'$	$Pm'm'n$
Raman tensor	$\begin{pmatrix} ae^{i\varnothing_a} & 0 & 0 \\ 0 & be^{i\varnothing_b} & 0 \\ 0 & 0 & ce^{i\varnothing_c} \end{pmatrix}$	$\begin{pmatrix} ae^{i\varnothing_a} & 0 & 0 \\ 0 & be^{i\varnothing_b} & -ide^{-i\varnothing_d} \\ 0 & ide^{i\varnothing_d} & ce^{i\varnothing_c} \end{pmatrix}$	$\begin{pmatrix} ae^{i\varnothing_a} & 0 & -ide^{-i\varnothing_d} \\ 0 & be^{i\varnothing_b} & 0 \\ ide^{i\varnothing_d} & 0 & ce^{i\varnothing_c} \end{pmatrix}$	$\begin{pmatrix} ae^{i\varnothing_a} & -ide^{-i\varnothing_d} & 0 \\ ide^{i\varnothing_d} & be^{i\varnothing_b} & 0 \\ 0 & 0 & ce^{i\varnothing_c} \end{pmatrix}$

A_g^1 branch is the most dispersive one, which explains the large separation between the A_g^1 and A_g^{1Z} modes, and the A_g^2 and A_g^3 branches are nearly flat, leading to the overlap of the zone-folding phonons and the original phonons.

Whether the zone-folding effects of the Raman modes appear depends on the symmetry of the magnetic configuration and the distortion pattern of the phonon mode. It is obvious that the FM state does not manifest zone-folding effects since it shares the same unit cell as the nonmagnetic primitive cell. For the AFM ground state, although the magnetic unit cell is doubled with respect to the primitive cell, the zone-folding effect for the Raman mode should still be absent. This is because the AFM state has a magnetic space group of P_anma, which has a symmetry operation element of $T\tau_{c/2}$. In other words, the neighboring layers in the magnetic unit cell are related simply by time-reversal operation T in the plane. However, the Raman scattering process is insensitive to the in-plane time-reversal operation for our backscattering measurement configuration. Therefore, in the Raman process, the two CrSBr layers in the AFM cell are indistinguishable and the Raman scattering dipole should be canceled for the zone-folding phonon mode of the two CrSBr layers. This is confirmed by our experiment and theoretical calculations (Supporting Information, S15).

When spin canting is involved under an external magnetic field, the Raman zone-folding effects depend on the direction of the canting direction. Experimentally, we observed that the zone-folding Raman modes appear for the magnetic field along the *a* axis (Figure 3), while they are absent for the magnetic field along the *c* axis (Supporting Information, S17). To understand the underlying mechanism, we examined the detailed vibrational modes and the symmetry operation elements of the magnetic space group (MSG) of the two canting states, i.e., the AFMy-FMx (MSG $Pc'cn'$) and the AFMy-FMz (MSG $Pnm'a'$) states. By examining the allowed symmetry operation elements, the vibrational patterns of the A_g modes are symmetric under the MSG operation element $\{C_{2x}||\tau_{(0,1/2,1/2)}\}$ for the AFMy-FMx state while antisymmetric under the $\{C_{2z}||\tau_{(0,0,1/2)}\}$ operation for the AFMy-FMz state (see detailed discussion in the Supporting Information, S18). In this sense, the zone-folding Raman modes are B_g (symmetric) modes and Raman-active for the magnetic field along the *a* axis, while these modes become B_u (antisymmetric) for the magnetic field along the *c* axis, which is Raman-inactive.

Previous magneto-Raman studies in CrI_3[28] and VI_3[29] demonstrated that the magnetic order (especially FM) displays a significant impact on the Raman scattering polarization of phonons, which is generally characterized by the Raman tensor. By using the magnetic space group analysis, here, we derive the Raman tensors for bulk CrSBr at the AFM and spin-polarized FM (the spins polarized along the *a*, *b*, and *c* axes and labeled as FM-*a*, FM-*b*, and FM-*c*, respectively) states, as listed in Table 1. The phase components in the Raman tensors are from the intrinsic optical anisotropy of CrSBr,[45] and the antisymmetric imaginary off-diagonal terms originate from the FM magnetic order.[28,46] To probe these off-diagonal terms, we measured the circular polarization-resolved Raman spectra for bulk CrSBr by applying the magnetic field along the *c* axis. Figure 4a displays the representative Raman spectra of bulk

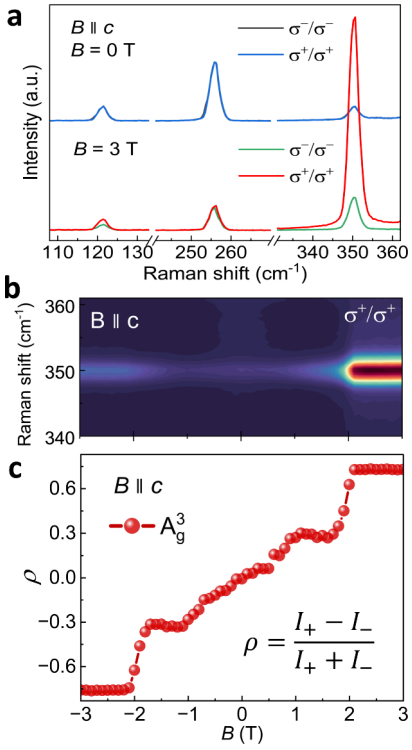

Figure 4. Circular polarization-resolved Raman spectra of bulk CrSBr under the magnetic field along the *c* axis. (a) Raman spectra from both σ^+/σ^+ and σ^-/σ^- channels at 0 (top panel) and 3 T (down panel). (b) Raman spectrum of the A_g^3 mode from the σ^+/σ^+ channel as a function of the magnetic field. (c) Degree of circular polarization (ρ) of the A_g^3 mode as a function of the magnetic field.

CrSBr at 0 and 3 T in the σ^+/σ^+ and σ^-/σ^- channels. At 0 T, all three A_g modes display identical intensities in the σ^+/σ^+ and σ^-/σ^- channels, which is consistent with the Raman tensor for the AFM CrSBr. After CrSBr is polarized into the FM-*c* state, we observe a significant intensity difference in two channels for the A_g^3 mode and a minor difference for the other two modes, which originates from the off-diagonal terms in the Raman tensor and is direct evidence for the time-reversal symmetry breaking. The evolution of the Raman spectra of the A_g^3 mode in the σ^+/σ^+ channel with the magnetic field is shown in Figure 4b, and the corresponding degree of circular polarization (DCP) is plotted in Figure 4c, where the DCP is defined as $\rho = \frac{I_+ - I_-}{I_+ + I_-}$, and the I_+ and I_- denote the intensities from the σ^+/σ^+ and σ^-/σ^- channels, respectively.

To further confirm the Raman tensors that we derived, the polarization-resolved Raman measurements are performed on

https://doi.org/10.1021/acsnano.5c13065
ACS Nano 2026, 20, 2655−2663

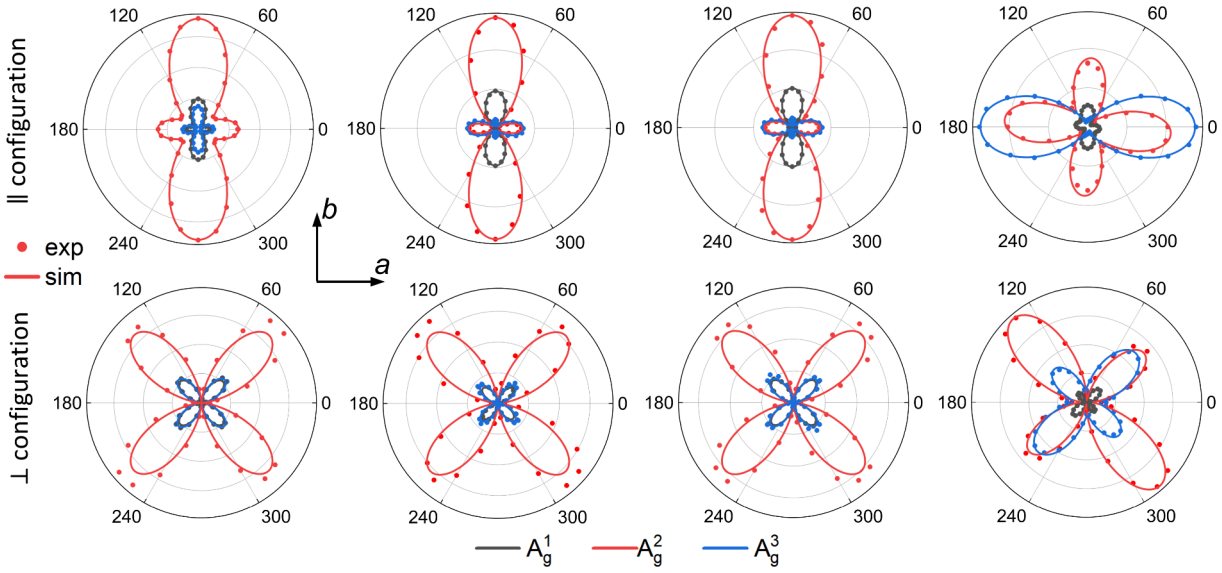

Figure 5. Polarization angle-dependent Raman intensities of the A_g modes from both XX and XY channels for bulk CrSBr at the AFM and FM-*a*, FM-*b*, and FM-*c* states. The polarization angle is defined as the angle between the polarization of the excitation light and the *a* axis.

bulk CrSBr at the AFM and polarized FM-*a*, FM-*b*, and FM-*c* states, and the Raman intensities of the A_g modes from both XX ($I^{\parallel}$) and XY ($I^{\perp}$) channels are summarized in Figure 5. The polarization angle dependences of the Raman intensities are calculated based on the Raman tensors (details are provided in the Supporting Information, S19). The results are used to fit the experimental data and match very well, as shown in Figure 5. Obviously, the polarization patterns for the AFM and FM-*a* and FM-*b* are very similar because the polarizations of the excitation and scattering lights are limited in the plane in our measurement configuration, and their Raman tensors are essentially the same. However, the polarization patterns for the FM-*c* are dramatically different due to the off-diagonal terms in the Raman tensor, which originated from the magnetic order. In addition, we note that for the AFM, FM-*a*, and FM-*b* spin configurations, the intensity polar plots are symmetric along the *a* and *b* axes, while for the FM-*c* case, this symmetry is broken, which is due to the breaking of mirror symmetries along both *a* and *b* axes in the FM-*c* state.

CONCLUSIONS

In conclusion, we have systematically studied the effect of the magnetic order on the Raman spectra of CrSBr. Due to the resonance effect, the Raman intensities of phonons display distinct dependence on the magnetic order for bulk and few-layer CrSBr, and even the metastable intermediate magnetic states in 3L and 4L samples can be easily resolved, which makes Raman spectroscopy an effective tool to probe the detailed spin textures in CrSBr. In addition, we observed strong zone-folding phonon modes from the A_g mode branches at the *a*-axis spin-canted states, and these modes are Raman-inactive at AFM, FM, and *c*-axis states due to the symmetry. Furthermore, we derived the Raman tensors of the A_g modes based on the magnetic space group analysis, and the off-diagonal terms that originated from the FM magnetic order show a dramatic impact on the scattering light polarization patterns of the phonon modes. Our work demonstrates profound influence of the magnetic order on the Raman spectra of CrSBr and highlights CrSBr as a unique platform for exploring novel magneto-optical effects.

METHODS

Sample Preparation

CrSBr crystals were synthesized by the chemical vapor transport method using the recipe described in ref 21. Bulk CrSBr flakes were mechanically exfoliated onto 285 nm SiO_2/Si substrates in an argon-filled glovebox, the selected thin-layer samples were encapsulated by hBN flakes using the dry transfer technique to prevent oxygen and moisture, and their thickness can be identified by magneto-PL spectroscopy.

Cryogenic Magneto-Optical Spectroscopy

Both cryogenic Raman and photoluminescence (PL) measurements were performed in a closed-cycle cryostat (attoDRY 2100) with 9/3 T superconducting vector magnets at 1.7 K. A 632.8 nm HeNe laser was used as the excitation source, and the power was kept below 150 μW. The spot size is roughly 2−3 μm on the sample. The backscattering light was collected by a spectrometer with 1800 grooves/mm grating and 3 mm slit width for most Raman measurements, except in Figure 3b, where the slit width was adjusted to 1 mm to improve dispersion resolution. For PL measurements, the grating was set to 600 grooves/mm. In angular-dependent polarized Raman measurements, the half (quarter)-wave plate was used to control the polarization (helicity) of incident light, and the linear polarizer was used to select the colinear or cross-linear component of scattered light. For the magneto-Raman experiments, the Faraday rotation was corrected with our half-wave plate (Supporting Information, S3).

First-Principles Calculations

Density functional theory (DFT) calculations were performed using the Vienna Ab initio Simulation Package[47] (VASP) to elucidate the phonon and electronic properties of CrSBr under various magnetic configurations. The projector-augmented wave (PAW) potentials were employed,[48] explicitly treating the valence electrons with configurations of $3d^5 4s^1$ for Cr, $3s^2 3p^4$ for S, and $4s^2 4p^5$ for Br. Exchange-correlation interactions were described using the Perdew−Burke−Ernzerhof functional optimized for solids (PBEsol).[49] To accurately capture van der Waals interactions between layers, the DFT-D3 scheme proposed by Grimme with zero damping was applied.[50]

Structural relaxations were carried out until the residual atomic forces were below 1 meV/Å. A Γ-centered Monkhorst−Pack k-point grid with a dense resolution of 0.02 (in units of 2π/Å) was adopted for Brillouin zone sampling, ensuring high precision in electronic and phonon band structures.

https://doi.org/10.1021/acsnano.5c13065
ACS Nano 2026, 20, 2655−2663

Phonon dispersion calculations were conducted using the finite-displacement method within the PHONOPY package[51,52] interfaced with VASP. To investigate magnetic-order-dependent phonon behavior, we explicitly considered different spin configurations, including AFM and FM structures. Magnetic configurations and their associated symmetry properties were systematically analyzed in the framework of magnetic space group theory, enabling the identification of Raman-active phonon modes and their evolution under external magnetic fields.

■ ASSOCIATED CONTENT

Supporting Information

The Supporting Information is available free of charge at https://pubs.acs.org/doi/10.1021/acsnano.5c13065.

Optical microscopy images; magneto-PL of CrSBr; compensation for Faraday rotation; temperature-dependent Raman spectra; magneto-Raman spectra of 1L CrSBr; circular polarization-resolved Raman spectra of 1L CrSBr; magnetic-order-dependent Raman spectra; magneto-Raman spectra with light polarized along the *a* axis; magneto-Raman spectra using 488 and 532 nm lasers; magneto-Raman spectra of B_g and multiple-phonon modes; zone-folding phonons with light polarized along the *b* axis; frequency shift of zone-folding phonons; density functional theory calculations; phonon band structure; calculated zone-folding phonon modes and A_g mode intensity; magnetic space group and Raman tensors for spin-canting configuration; Raman spectra of *c*-axis canting CrSBr; symmetry analysis of the spin-canting states; the angular dependence of the polarized Raman intensity (PDF)

■ AUTHOR INFORMATION

Corresponding Author

Mingyuan Huang − *Department of Physics, State Key Laboratory of Quantum Functional Materials, and Guangdong Basic Research Center of Excellence for Quantum Science and Guangdong Provincial Key Laboratory of Advanced Thermoelectric Materials and Device Physics, Southern University of Science and Technology, Shenzhen 518055, China;* orcid.org/0000-0002-3901-6451; Email: huangmy@sustech.edu.cn

Authors

Junyang Chen − *Department of Physics, State Key Laboratory of Quantum Functional Materials, and Guangdong Basic Research Center of Excellence for Quantum Science, Southern University of Science and Technology, Shenzhen 518055, China*

Mingqiang Gu − *Department of Physics, State Key Laboratory of Quantum Functional Materials, and Guangdong Basic Research Center of Excellence for Quantum Science, Southern University of Science and Technology, Shenzhen 518055, China; School of Flexible Electronics (SoFE) & State Key Laboratory of Optoelectronic Materials and Technologies (OEMT), Sun Yat-sen University, Shenzhen, Guangdong 518107, P. R. China; Institute of Materials Engineering, Nanjing University, Jiangsu, Nantong 226019, P.R. China*

Xiaohua Wu − *Department of Physics, State Key Laboratory of Quantum Functional Materials, and Guangdong Basic Research Center of Excellence for Quantum Science, Southern University of Science and Technology, Shenzhen 518055, China*

Shoujing Chen − *Department of Physics, State Key Laboratory of Quantum Functional Materials, and Guangdong Basic Research Center of Excellence for Quantum Science, Southern University of Science and Technology, Shenzhen 518055, China*

Guangji Xing − *Department of Physics, State Key Laboratory of Quantum Functional Materials, and Guangdong Basic Research Center of Excellence for Quantum Science, Southern University of Science and Technology, Shenzhen 518055, China*

Mengyuan Jia − *Department of Physics, State Key Laboratory of Quantum Functional Materials, and Guangdong Basic Research Center of Excellence for Quantum Science, Southern University of Science and Technology, Shenzhen 518055, China*

Tiejun Huang − *Department of Physics, State Key Laboratory of Quantum Functional Materials, and Guangdong Basic Research Center of Excellence for Quantum Science, Southern University of Science and Technology, Shenzhen 518055, China*

Hao Peng − *Department of Physics, State Key Laboratory of Quantum Functional Materials, and Guangdong Basic Research Center of Excellence for Quantum Science, Southern University of Science and Technology, Shenzhen 518055, China*

Minghong Sun − *Department of Physics, State Key Laboratory of Quantum Functional Materials, and Guangdong Basic Research Center of Excellence for Quantum Science, Southern University of Science and Technology, Shenzhen 518055, China*

Qihang Liu − *Department of Physics, State Key Laboratory of Quantum Functional Materials, and Guangdong Basic Research Center of Excellence for Quantum Science, Southern University of Science and Technology, Shenzhen 518055, China; Quantum Science Center of Guangdong−Hong Kong−Macao Greater Bay Area (Guangdong), Shenzhen 518045, China; Guangdong Provincial Key Laboratory for Computational Science and Material Design, Southern University of Science and Technology, Shenzen, Guangdong 518045, China;* orcid.org/0000-0001-9843-2482

Yanan Dai − *Department of Physics, State Key Laboratory of Quantum Functional Materials, and Guangdong Basic Research Center of Excellence for Quantum Science and Guangdong Provincial Key Laboratory of Advanced Thermoelectric Materials and Device Physics, Southern University of Science and Technology, Shenzhen 518055, China; Quantum Science Center of Guangdong−Hong Kong−Macao Greater Bay Area (Guangdong), Shenzhen 518045, China;* orcid.org/0000-0002-0192-1480

Complete contact information is available at: https://pubs.acs.org/10.1021/acsnano.5c13065

Author Contributions

‡J.C. and M.G. contributed equally to this work. J.C. fabricated the sample devices and performed the experiments with the help of X.W., G.X., T.H., and H.P. M.H. supervised the project. M.G. and Q.L. performed the theoretical analysis and DFT calculations. J.C. and M.H. drafted and revised the manuscript with the help of Y.D. and S.C. All authors contributed to the scientific discussion.

Notes

The authors declare no competing financial interest.

https://doi.org/10.1021/acsnano.5c13065
ACS Nano 2026, 20, 2655−2663

■ ACKNOWLEDGMENTS

This work was supported by the National Natural Science Foundation of China (grant nos. 12074165 and 12474232), Guangdong Provincial Key Laboratory of Advanced Thermoelectric Materials and Device Physics (grant no. 2024B1212010001), and the Shenzhen Science and Technology Program (grant no. 20231117151322001).

■ REFERENCES

(1) Burch, K. S.; Mandrus, D.; Park, J.-G. Magnetism in two-dimensional van der Waals materials. *Nature* **2018**, *563*, 47−52.
(2) Chen, W.; Sun, Z.; Wang, Z.; Gu, L.; Xu, X.; Wu, S.; Gao, C. Direct observation of van der Waals stacking−dependent interlayer magnetism. *Science* **2019**, *366*, 983−987.
(3) Deng, Y.; Yu, Y.; Song, Y.; Zhang, J.; Wang, N. Z.; Sun, Z.; Yi, Y.; Wu, Y. Z.; Wu, S.; Zhu, J. Gate-tunable room-temperature ferromagnetism in two-dimensional Fe3GeTe2. *Nature* **2018**, *563*, 94−99.
(4) Fei, Z.; Huang, B.; Malinowski, P.; Wang, W.; Song, T.; Sanchez, J.; Yao, W.; Xiao, D.; Zhu, X.; May, A. F. Two-dimensional itinerant ferromagnetism in atomically thin Fe3GeTe2. *Nat. Mater.* **2018**, *17*, 778−782.
(5) Gong, C.; Li, L.; Li, Z.; Ji, H.; Stern, A.; Xia, Y.; Cao, T.; Bao, W.; Wang, C.; Wang, Y. Discovery of intrinsic ferromagnetism in two-dimensional van der Waals crystals. *Nature* **2017**, *546*, 265−269.
(6) Gong, C.; Zhang, X. Two-dimensional magnetic crystals and emergent heterostructure devices. *Science* **2019**, *363*, No. eaav4450.
(7) Huang, B.; Clark, G.; Navarro-Moratalla, E.; Klein, D. R.; Cheng, R.; Seyler, K. L.; Zhong, D.; Schmidgall, E.; McGuire, M. A.; Cobden, D. H. Layer-dependent ferromagnetism in a van der Waals crystal down to the monolayer limit. *Nature* **2017**, *546*, 270−273.
(8) Klein, D. R.; MacNeill, D.; Lado, J. L.; Soriano, D.; Navarro-Moratalla, E.; Watanabe, K.; Taniguchi, T.; Manni, S.; Canfield, P.; Fernández-Rossier, J. Probing magnetism in 2D van der Waals crystalline insulators via electron tunneling. *Science* **2018**, *360*, 1218−1222.
(9) Song, T.; Cai, X.; Tu, M. W.-Y.; Zhang, X.; Huang, B.; Wilson, N. P.; Seyler, K. L.; Zhu, L.; Taniguchi, T.; Watanabe, K. Giant tunneling magnetoresistance in spin-filter van der Waals heterostructures. *Science* **2018**, *360*, 1214−1218.
(10) Zhong, D.; Seyler, K. L.; Linpeng, X.; Wilson, N. P.; Taniguchi, T.; Watanabe, K.; McGuire, M. A.; Fu, K.-M. C.; Xiao, D.; Yao, W. Layer-resolved magnetic proximity effect in van der Waals heterostructures. *Nat. Nanotechnol.* **2020**, *15*, 187−191.
(11) Cheng, G.; Rahman, M. M.; He, Z.; Allcca, A. L.; Rustagi, A.; Stampe, K. A.; Zhu, Y.; Yan, S.; Tian, S.; Mao, Z. Emergence of electric-field-tunable interfacial ferromagnetism in 2D antiferromagnet heterostructures. *Nat. Commun.* **2022**, *13*, 7348.
(12) Deng, Y.; Yu, Y.; Shi, M. Z.; Guo, Z.; Xu, Z.; Wang, J.; Chen, X. H.; Zhang, Y. Quantum anomalous Hall effect in intrinsic magnetic topological insulator MnBi2Te4. *Science* **2020**, *367*, 895−900.
(13) Song, T.; Sun, Q.-C.; Anderson, E.; Wang, C.; Qian, J.; Taniguchi, T.; Watanabe, K.; McGuire, M. A.; Stöhr, R.; Xiao, D. Direct visualization of magnetic domains and moiré magnetism in twisted 2D magnets. *Science* **2021**, *374*, 1140−1144.
(14) Xie, H.; Luo, X.; Ye, G.; Ye, Z.; Ge, H.; Sung, S. H.; Rennich, E.; Yan, S.; Fu, Y.; Tian, S. Twist engineering of the two-dimensional magnetism in double bilayer chromium triiodide homostructures. *Nat. Phys.* **2022**, *18*, 30−36.
(15) Xu, Y.; Ray, A.; Shao, Y.-T.; Jiang, S.; Lee, K.; Weber, D.; Goldberger, J. E.; Watanabe, K.; Taniguchi, T.; Muller, D. A. Coexisting ferromagnetic−antiferromagnetic state in twisted bilayer CrI3. *Nat. Nanotechnol.* **2022**, *17*, 143−147.
(16) Huang, B.; Clark, G.; Klein, D. R.; MacNeill, D.; Navarro-Moratalla, E.; Seyler, K. L.; Wilson, N.; McGuire, M. A.; Cobden, D. H.; Xiao, D. Electrical control of 2D magnetism in bilayer CrI 3. *Nat. Nanotechnol.* **2018**, *13*, 544−548.
(17) Zhong, D.; Seyler, K. L.; Linpeng, X.; Cheng, R.; Sivadas, N.; Huang, B.; Schmidgall, E.; Taniguchi, T.; Watanabe, K.; McGuire, M. A. Van der Waals engineering of ferromagnetic semiconductor heterostructures for spin and valleytronics. *Sci. Adv.* **2017**, *3*, No. e1603113.
(18) Telford, E. J.; Dismukes, A. H.; Dudley, R. L.; Wiscons, R. A.; Lee, K.; Chica, D. G.; Ziebel, M. E.; Han, M.-G.; Yu, J.; Shabani, S. Coupling between magnetic order and charge transport in a two-dimensional magnetic semiconductor. *Nat. Mater.* **2022**, *21*, 754−760.
(19) Telford, E. J.; Dismukes, A. H.; Lee, K.; Cheng, M.; Wieteska, A.; Bartholomew, A. K.; Chen, Y. S.; Xu, X.; Pasupathy, A. N.; Zhu, X. Layered antiferromagnetism induces large negative magnetoresistance in the van der Waals semiconductor CrSBr. *Adv. Mater.* **2020**, *32*, 2003240.
(20) Wu, F.; Gutiérrez-Lezama, I.; López-Paz, S. A.; Gibertini, M.; Watanabe, K.; Taniguchi, T.; von Rohr, F. O.; Ubrig, N.; Morpurgo, A. F. Quasi-1D electronic transport in a 2D magnetic semiconductor. *Adv. Mater.* **2022**, *34*, 2109759.
(21) Wilson, N. P.; Lee, K.; Cenker, J.; Xie, K.; Dismukes, A. H.; Telford, E. J.; Fonseca, J.; Sivakumar, S.; Dean, C.; Cao, T. Interlayer electronic coupling on demand in a 2D magnetic semiconductor. *Nat. Mater.* **2021**, *20*, 1657−1662.
(22) Klein, J.; Pingault, B.; Florian, M.; Heißenbüttel, M.-C.; Steinhoff, A.; Song, Z.; Torres, K.; Dirnberger, F.; Curtis, J. B.; Weile, M. The bulk van der Waals layered magnet CrSBr is a quasi-1D material. *ACS Nano* **2023**, *17*, 5316−5328.
(23) Bae, Y. J.; Wang, J.; Scheie, A.; Xu, J.; Chica, D. G.; Diederich, G. M.; Cenker, J.; Ziebel, M. E.; Bai, Y.; Ren, H. Exciton-coupled coherent magnons in a 2D semiconductor. *Nature* **2022**, *609*, 282−286.
(24) Diederich, G. M.; Cenker, J.; Ren, Y.; Fonseca, J.; Chica, D. G.; Bae, Y. J.; Zhu, X.; Roy, X.; Cao, T.; Xiao, D. Tunable interaction between excitons and hybridized magnons in a layered semiconductor. *Nat. Nanotechnol.* **2023**, *18*, 23−28.
(25) Dirnberger, F.; Quan, J.; Bushati, R.; Diederich, G. M.; Florian, M.; Klein, J.; Mosina, K.; Sofer, Z.; Xu, X.; Kamra, A. Magneto-optics in a van der Waals magnet tuned by self-hybridized polaritons. *Nature* **2023**, *620*, 533−537.
(26) Wang, T.; Zhang, D.; Yang, S.; Lin, Z.; Chen, Q.; Yang, J.; Gong, Q.; Chen, Z.; Ye, Y.; Liu, W. Magnetically-dressed CrSBr exciton-polaritons in ultrastrong coupling regime. *Nat. Commun.* **2023**, *14*, 5966.
(27) Nessi, L.; Occhialini, C. A.; Demir, A. K.; Powalla, L.; Comin, R. Magnetic Field Tunable Polaritons in the Ultrastrong Coupling Regime in CrSBr. *ACS Nano* **2024**, *18*, 34235−34243.
(28) Huang, B.; Cenker, J.; Zhang, X.; Ray, E. L.; Song, T.; Taniguchi, T.; Watanabe, K.; McGuire, M. A.; Xiao, D.; Xu, X. Tuning inelastic light scattering via symmetry control in the two-dimensional magnet CrI3. *Nature Nanotechnol.* **2020**, *15*, 212−216.
(29) Lyu, B.; Gao, Y.; Zhang, Y.; Wang, L.; Wu, X.; Chen, Y.; Zhang, J.; Li, G.; Huang, Q.; Zhang, N. Probing the ferromagnetism and spin wave gap in VI3 by helicity-resolved Raman spectroscopy. *Nano Lett.* **2020**, *20*, 6024−6031.
(30) Yin, T.; Ulman, K. A.; Liu, S.; Granados del Águila, A.; Huang, Y.; Zhang, L.; Serra, M.; Sedmidubsky, D.; Sofer, Z.; Quek, S. Y. Chiral phonons and giant magneto-optical effect in CrBr3 2D magnet. *Adv. Mater.* **2021**, *33*, 2101618.
(31) Tian, Y.; Gray, M. J.; Ji, H.; Cava, R. J.; Burch, K. S. Magneto-elastic coupling in a potential ferromagnetic 2D atomic crystal. *2D Materials* **2016**, *3*, No. 025035.
(32) McCreary, A.; Mai, T. T.; Utermohlen, F. G.; Simpson, J. R.; Garrity, K. F.; Feng, X.; Shcherbakov, D.; Zhu, Y.; Hu, J.; Weber, D. Distinct magneto-Raman signatures of spin-flip phase transitions in CrI3. *Nat. Commun.* **2020**, *11*, 3879.
(33) Padmanabhan, H.; Poore, M.; Kim, P. K.; Koocher, N. Z.; Stoica, V. A.; Puggioni, D.; Wang, H.; Shen, X.; Reid, A. H.; Gu, M. Interlayer magnetophononic coupling in MnBi2Te4. *Nat. Commun.* **2022**, *13*, 1929.

https://doi.org/10.1021/acsnano.5c13065
ACS Nano 2026, 20, 2655−2663

(34) Torres, K.; Kuc, A.; Maschio, L.; Pham, T.; Reidy, K.; Dekanovsky, L.; Sofer, Z.; Ross, F. M.; Klein, J. Probing Defects and Spin-Phonon Coupling in CrSBr via Resonant Raman Scattering. *Adv. Funct. Mater.* **2023**, *33*, 2211366.
(35) Pawbake, A.; Pelini, T.; Wilson, N. P.; Mosina, K.; Sofer, Z.; Heid, R.; Faugeras, C. Raman scattering signatures of strong spin-phonon coupling in the bulk magnetic van der Waals material CrSBr. *Phys. Rev. B* **2023**, *107*, No. 075421.
(36) Mondal, P.; Markina, D. I.; Hopf, L.; Krelle, L.; Shradha, S.; Klein, J.; Glazov, M. M.; Gerber, I.; Hagmann, K.; Klitzing, R. v. Raman polarization switching in CrSBr. *npj 2D Mater. Appl.* **2025**, *9*, 22.
(37) Sahu, S.; Berrezueta-Palacios, C.; Juergensen, S.; Mosina, K.; Sofer, Z.; Velický, M.; Kusch, P.; Frank, O. Resonance Raman scattering and anomalous anti-Stokes phenomena in CrSBr. *Nanoscale* **2025**, *17*, 11539−11546.
(38) Shi, J.; Wang, D.; Jiang, N.; Xin, Z.; Zheng, H.; Shen, C.; Zhang, X.; Liu, X. Giant Magneto-Exciton Coupling in 2D van der Waals CrSBr. *ACS Nano* **2024**, *19* (33), 29977−29987.
(39) Li, C.; Shen, C.; Ma, X.; Jiang, N.; Song, J.; Tang, K. K.; Deng, X.; Guo, J.; Liu, X.; Zhang, Q.Strongly Magnetically Tuned Exciton-Polaritons in van der Waals CrSBr. *arXiv preprint arXiv:2411.11555***2024**. DOI: .
(40) Wu, X.; Chen, J.; Gu, M.; Zhang, Y.; Wang, S.; Dai, Y.; Liu, Q.; Zhao, Y.; Huang, M.Magnetic order dependent photoluminescence from high energy excitons in hBN protected few-layer CrSBr. *arXiv preprint arXiv:2507.23301***2025**. DOI: .
(41) Cenker, J.; Sivakumar, S.; Xie, K.; Miller, A.; Thijssen, P.; Liu, Z.; Dismukes, A.; Fonseca, J.; Anderson, E.; Zhu, X. Reversible strain-induced magnetic phase transition in a van der Waals magnet. *Nat. Nanotechnol.* **2022**, *17*, 256−261.
(42) Tabataba-Vakili, F.; Nguyen, H. P.; Rupp, A.; Mosina, K.; Papavasileiou, A.; Watanabe, K.; Taniguchi, T.; Maletinsky, P.; Glazov, M. M.; Sofer, Z. Doping-control of excitons and magnetism in few-layer CrSBr. *Nat. Commun.* **2024**, *15*, 4735.
(43) Sun, Z.; Hong, C.; Chen, Y.; Sheng, Z.; Wu, S.; Wang, Z.; Liang, B.; Liu, W.-T.; Yuan, Z.; Wu, Y. Resolving and routing magnetic polymorphs in a 2D layered antiferromagnet. *Nat. Mater.* **2025**, 1−8.
(44) Liu, Z.; Sun, Y.; Zhu, C.; Hong, C.; Gao, Y.; Sun, Z.; Watanabe, K.; Taniguchi, T.; Wu, S.; Chen, Z. Spin texture and tunneling magnetoresistance in atomically thin CrSBr. *Phys. Rev. B* **2025**, *111*, L140417.
(45) Pimenta, M. A.; Resende, G. C.; Ribeiro, H. B.; Carvalho, B. R. Polarized Raman spectroscopy in low-symmetry 2D materials: angle-resolved experiments and complex number tensor elements. *Phys. Chem. Chem. Phys.* **2021**, *23*, 27103−27123.
(46) Zhang, Y.; Wu, X.; Lyu, B.; Wu, M.; Zhao, S.; Chen, J.; Jia, M.; Zhang, C.; Wang, L.; Wang, X. Magnetic order-induced polarization anomaly of Raman scattering in 2D magnet CrI3. *Nano Lett.* **2019**, *20*, 729−734.
(47) Kresse, G.; Furthmüller, J. Efficiency of ab-initio total energy calculations for metals and semiconductors using a plane-wave basis set. *Computational materials science* **1996**, *6*, 15−50.
(48) Blöchl, P. E. Projector augmented-wave method. *Phys. Rev. B* **1994**, *50*, 17953.
(49) Perdew, J. P.; Burke, K.; Ernzerhof, M. Generalized gradient approximation made simple. *Physical review letters* **1996**, *77*, 3865.
(50) Grimme, S.; Antony, J.; Ehrlich, S.; Krieg, H.**2010**, A consistent and accurate ab initio parametrization of density functional dispersion correction (DFT-D) for the 94 elements H-Pu. *J. Chem. Phys.132*. DOI: .
(51) Togo, A.; Chaput, L.; Tadano, T.; Tanaka, I. Implementation strategies in phonopy and phono3py. *J. Phys.: Condens. Matter* **2023**, *35*, 353001.
(52) Togo, A. First-principles phonon calculations with phonopy and phono3py. *J. Phys. Soc. Jpn.* **2023**, *92*, No. 012001.

https://doi.org/10.1021/acsnano.5c13065
ACS Nano 2026, 20, 2655−2663